IEEE Access
Multidisciplinary | Rapid Review | Open Access Journal

Received October 10, 2020, accepted October 18, 2020, date of publication October 26, 2020, date of current version November 12, 2020.

Digital Object Identifier 10.1109/ACCESS.2020.3033826

Flat-Feet Prediction Based on a Designed Wearable Sensing Shoe and a PCA-Based Deep Neural Network Model

JUNG-YOON KIM[1], JA YOUNG HWANG[2], EUNSE PARK[3], HYEON-UK NAM[4], AND SONGHEE CHEON[5]

[1]Department of Computer Science, Kent State University, Kent, OH 44242, USA
[2]School of Fashion, Kent State University, Kent, OH 44242, USA
[3]Department of Physical Therapy, University of North Georgia, Dahlonega, GA 30579, USA
[4]CHA Gumi Medical Center, Department of Rehabilitation of Medicine, CHA University, Gumi 39295, South Korea
[5]Department of Physical Therapy, Youngsan University, Yangsan 50510, South Korea

Corresponding author: Songhee Cheon (1000sh@ysu.ac.kr)

This work was supported by the National Research Foundation of Korea (NRF) grant funded by the Korea government under Grant NRF-2017R1C1B5076194.

ABSTRACT Gait is a significant factor that affects human health, and monitoring a person's gait with sensing devices during daily life can detect abnormal gait events that affect numerous physical health problems. In particular, flat feet can cause changes in alignment conditions of the foot, ankle, leg, pelvis and spine. The primary problem with previous studies of wearable devices for measuring gait have focused on quantitatively monitoring the degree of gait rather than the limited gait ability. The existing method of feeding back the degree of gait or activity does not consider the severity of the subject and is insufficient for qualitative evaluation or training of gait. The significance of this study is development of convenient detecting and long-term tracking tools that can be used by both patients and clinicians for prescreening flat feet and monitoring the progress of flat feet treatment. For wearable devices for flatfoot detection to be most effective, detection systems and algorithms must be accurate, robust, reliable and computationally-efficient. In this paper, we developed an integrated smart wearable gait-monitoring device comprised of three sensors: front force, rear force, and an ankle flex sensor. We propose a new flat feet detection methodology based on a dynamic sensing window and a deep neural network with scaled principal component analysis (PCA). We tested 24 subjects, including both those with healthy gait and flat-feet-affected gait. Our study shows that the proposed sensing devices could be worn comfortably. The proposed deep neural network (DNN) model outperformed the other five classifier algorithms considered, and the area under the curve (AUC) value of the method was 87.1%. This wearable device can thus be easily and simply used both by patients and doctors to monitor the progress of flat feet and prescreen for possible gait problems in daily life.

INDEX TERMS DNN, wearable sensor, gait monitoring, multi-sensor, flatfoot, flexible sensor, force sensor, sock shoes.

I. INTRODUCTION

The individual walking characteristic called gait is considered an essential sign of human health and a useful biometric marker [1]–[3]. Among the factors affecting human gait, walking speed is a reasonable and sensitive measure for monitoring and assessing functional weakness and general health and, thus, gait speed is considered the sixth vital sign [1], [2]. Both functional and physiological changes in gait are indicative and predictive of various health-related factors, including the response to rehabilitation, mobility disability, falls, and cognitive decline [2]. Negative progression of gait is connected to clinical changes in life quality and health conditions [4]. Therefore, continuous and natural monitoring of gait during daily life, rather than during a hospital or clinical examination, can provide diverse information related to an individual's health.

Flatfoot, also called pes planus or fallen arches, is a postural deformity in which the arches of the foot are collapsed and the entire sole of the foot lays against the ground, either

The associate editor coordinating the review of this manuscript and approving it for publication was Xiong Luo.

completely or nearly completely. The structure of flatfoot is related to the biomechanics of the lower leg and affects its functionality. The arch provides flexibility and springiness between the forefoot and the hindfoot, allowing weight forces on the foot to be distributed in a way that minimizes negative effects on the bones of the leg and thigh [5]. Flatfoot can cause conditions related to the alignment of the foot, ankle, leg, pelvis and spine. Since these foot conditions are unstable, related joints experience excessive and unusual movements, and may become easily tired or damaged. In the long term, flatfoot can also cause numerous health problems, such as joint inflammation, hallux valgus, heel pain syndrome, interdigital neuroma, diverse foot deformities and pain. In addition, to correct foot instability, the tibialis anterior becomes too strongly involved, which may lead to shin splints, causing pain at the front of the shin. Such flat feet require a functional foot brace based on medical diagnosis to avoid progression of complex foot abnormality [6], [7].

A visual assessment based on an optical motion capture system or force plate is the gold standard for examining gait events. Such monitoring systems are expensive, large, and only able to measure human gait within a limited space. They are limited to clinical usage or research and are not sufficiently convenient and comfortable enough for use in normal living environments. The use of alternative sensors for capturing gait events, such as foot switch or force sensitive resistors [8]–[11], air pressure sensors [12], [13], Wi-Fi signals as a gait sensor [4], accelerometer sensors [14]–[18] and inertial measurement unit sensors [9], [19]–[35] has been studied. However, these methodologies have several limitations caused by their sensing characteristics. Although force sensors and inertial measurement unit (IMU) sensors including the accelerometer, gyroscope and magnetometer are widely considered practical alternatives, they are unable to measure the detailed ankle movements related to flatfoot events. A miniaturized IMU sensor makes single-point measurement possible for estimation of gait problems. However, flatfoot events are somewhat difficult to detect using such sensors. Therefore, we include a flexible sensor on the human ankle to measure the detailed angles of foot movement directly.

In this paper, we present an integrated wearable gait monitoring system that can detect an individual's flatfoot events using a combination of flexible and force sensors with data processing via deep neural network classification, employing gait data from 24 subjects. The proposed methodology automatically extracts data segments based on front and rear force sensors, so that the user is not required to keep walking on a designated path but, instead, can freely walk in an open space. It will automatically filter non-gait data, extract gait-related features and detect flatfoot events. The proposed data analysis of gait signals consists of three data processing modules, including 1) segmentation of one gait cycle, 2) flatfoot-related feature extraction, and 3) classification module for detection of flatfoot events. The segmentation of one gait cycle must capture the exact timing and intervals of heel strikes. In general, the interval from heel strike to heel strike is considered one gait cycle, so we used the front and rear force sensors as inputs and recorded the sequential activation of sensors. Flatfoot-related features can be extracted by the flexible sensor, reflecting the ankle movements that occur throughout the gait cycle. The classification module for detecting flatfoot events uses scaled PCA and a deep neural network.

The present study makes the following contributions:

1) Design of a new type of wearable sock shoe that is comfortable and provides flexibility and adaptability for individuals with unique or unusual foot shapes.
2) Development of a sensing device to measure gait cycles and ankle movements based on the integration of force and flexible sensors.
3) Development of a feature-extraction algorithm for generating 12 features based on combination of three different sensor signals and building classification algorithms for detecting flat feet events based on the extracted features.
4) A prototype of the proposed integrated system was implemented and tested for experiments in typical indoor spaces.

The results demonstrated the accuracy and comfort of the wearable device for continuous use. The paper is organized as follows. Related work is described in Section 2. The proposed flat feet detection system is introduced in Section 3, followed by results and discussion in Section 4. Our conclusions are provided in Section 5.

II. RELATED WORK

A. FLATFOOT DIAGNOSIS

Flatfoot is defined as a dynamic deformity, which involves flattening of the medial arch. This deformity may originate from both posterior tibial tendon insufficiency and failure of the capsular and ligamentous structures of the foot [36]. The gold standard for evaluating adult flatfoot is the weight-bearing radiograph. Radiographic evaluation requires views from all possible directions, i.e., the anteroposterior, lateral, and hindfoot views. The images were evaluated by assessing the degree of arch collapse by measuring the first tarsometatarsal lateral angle and forefoot abduction at the talonavicular joint [37]. Based on the radiological images, four stages of flatfoot have been proposed to classify the severity of flatfoot (Table 1) [38], [39]. Magnetic resonance imaging (MRI) [40] is considered a useful tool for diagnosis of flatfoot and planning of surgical procedures. Some studies have indicated that ultrasound may be more useful for assessing the posterior tibial tendon than MRI, which is more time consuming and expensive [41]. Clinical assessment and examination, however, is the most widely used to identify the deformity because it is relatively reliable and diagnostic convenient. The Hübscher maneuver (Jack's test) is a functional test to evaluate the flexibility of flatfoot. The test is performed with the patient weight bearing on the foot flat, while the clinician dorsiflexes the hallux and watches for decreasing of

TABLE 1. Stages of flatfoot.

Stage	Description
I	No deformity (preexisting relative flatfoot often present)
IIa	Moderate flexible deformity (minimal abduction through talonavicular joint, <30% talonavicular uncoverage)
IIb	Severe flexible deformity with either abduction deformity through talonavicular joint (i.e., >30%-40% talonavicular uncoverage) or subtalar impingement
III	Fixed deformity (involving the triple-joint complex) Hindfoot valgus and flexible ankle valgus without significant
IVa	ankle arthritis
IVb	Hindfoot valgus with rigid ankle valgus or flexible deformity with significant ankle arthritis

the arch. Jack's test can differentiate between dynamic (flexible) flatfoot and static (rigid) flatfoot [42]. Navicular drop test is widely used in clinical settings and considered as a reproducible, valid and simple test to evaluate foot arch compare to the other tests using footprint parameters. This test is statistically significant in providing correlation to the actual arch angle [43].

Flatfoot deformity is related to changes in mobility and postural stability. Flatfoot causes failure of foot locking and reduced propulsive force during the gait cycle, which can increase the risk of falls [44], [45]. It has been reported that the flatfoot-affected population shows a significant decrease in gait cadence, speed, stride length, and step width. In addition, hindfoot abduction in the terminal stance and pre-swing phase is lost [46]. This deformity not only generates abnormal foot pressure during walking, but is also linked to injury possibility and the development of frequent pain [47].

B. DESIGN OF THE WEARABLE DEVICE

Designing wearable sensing system shoes requires a mix of creativity and practical design to develop a stylish and functional item. Understanding the potential needs of users when designing wearable technologies is essential. According to Ferraro and Ugur (2011), ''Wearability means ability to wear and concern the physical shape of wearables and their active relationship with the human form.'' (pg. 3) [48]. Wearable items act as a second skin outside of the body, providing protection based on their shape and form. Therefore, when designing wearable technologies, it is essential to understand the interactions between the human body and the wearable object, and to use flexible shapes that do not interrupt human motion. Therefore, shoes must fit appropriately and comfortably to facilitate adoption of the shoes by consumers and maximize the benefits to an individual's mobility.

The Institute of Complex Engineered Systems (ICES) suggests that designers should consider five wearability parameters when designing wearable products: a) attachment, b) size, c) human movement, d) unobtrusiveness, and e) body motion. According to the ICES, the top of the foot is an unobtrusive area [48]. The study of non-obtrusive shapes and their adaptation to the contours of the foot is critical when designing shoes. In addition, when developing a wearable object, comfort, adaptableness to varying forms of the foot, and the relationship between the wearable and the foot are vital aspects that must be considered [48]. Thus, important factors in the design of wearable shoes are functionality, wearability, comfort and fashion. Moreover, the design should be attractive to wearers from all age groups and communities.

III. DESIGN OF THE PROPOSED WEARABLE SHOE

The starting point of this project was the necessity for wearable technology to be available to consumers. During the initial phase, we employed an interdisciplinary team of a fashion designer, engineers, a customer, and a medical professional, who were tasked with identifying design issues. Each customer has a different heel shape and foot width. In addition, feet swell at the end of the day, and this effect is stronger in individuals with flat feet than in those without flat feet. However, shoes that are currently on the market do not address the needs of consumers. The optimal shoes for flat feet depend on the person's gait cycle, range of motion, and individual foot characteristics. The design proposed here focuses on resolving the issues of fit and comfort for consumers. To deal with functional abilities, the designer considered the movements, posture, and physical state of the consumer to develop ergonomic and enveloping shapes for the foot. Not only is the technical aspect of shoe design important but the aesthetics of shoe design are also crucial, as consumers will be hesitant to buy a product if its design is unsatisfactory. A design that embraces aesthetic concerns and considers customer needs will also meet the demands of human anatomy and support activity by the user.

The footwear industry has adopted various textiles and materials to improve the areas of fit, comfort, and functionality. One recent design trend in the athletic footwear market is that of knitted shoe uppers. Our design originated from a knit sock. A sock is an item of clothing worn on the foot and ankle. It provides protection from temperature changes and injury while absorbing sweat to keep feet dry and free from fungal growth. In ancient times, socks were made from leather or matted hair, while today, machine knitting is the predominant method used to satisfy the ready-to-wear industry. A knit sock will adapt to any foot shape to fit perfectly. Therefore, we applied the concept of a knit sock to our wearable shoe and designed a knit sock-style shoe with a flat wedge heel that can be pulled on or slipped on. Knit shoes allow placement of a flexible sensing device at the ankle. For this reason, the designer selected four-way stretch knit, which is sufficiently flexible to adapt to the anatomy of the feet. The sock shoes provide flexibility and adaptability for individuals with unique or unusual foot shapes. Fig. 1 shows the wearable gait monitoring shoe (WGMS) designed here with the positions of three sensors and the embedded system.

IV. THE PROPOSED SENSING ENVIRONMENT

Fig. 2 shows an overall system diagram and data flow of the proposed system. The WGMS consists of an embedded

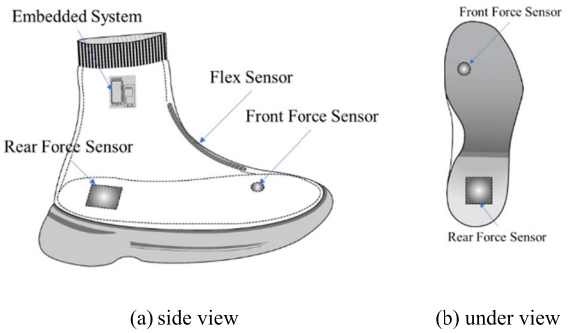

FIGURE 1. Physical layout of the wearable sensing shoe.

FIGURE 2. Overall system diagram and data flow of the gait monitoring system developed for detection of flatfoot.

system device, two force sensors and a flexible sensor. This wearable shoe measures gait-related signals and transmits the raw signals to a smart phone through Bluetooth communication. The sampling rates of the signals are 100 Hz, so the rate of data from the sensing device to the smart phone is 600 bytes per second (2 bytes $\times$ 100 Hz $\times$ 3 sensing signals). The smart phone performs initial window segmentation to extract the 12 initial feature data, sent to a computer through Wi-Fi or LTE communication. Since the initial feature data transmission occurs at every gait cycle, the amount of data that needs to be transferred over LTE or WiFi for a typical use case varies with the individual person. Murray, *et al.*, 1964 stated, ''The average duration of one gait cycle for men ranges from 0.98 to 1.07 seconds''. We can thus determine the transferred amount of 12 floating-point data ranges between 28.57 bytes / seconds (28 byte / 0.98s) and 26.17 (28 byte / 1.07s). In the computer, diverse-data processing modules, including feature extraction, scaled PCA, and classification based on the deep neural network (DNN) are executed to detect flat feet events. After processing, the results are sent back to the smart phone to provide feedback to the user.

A. SENSING DEVICE

The sensing system is illustrated in Fig. 3. Direct current (DC) is applied to the force and flexible sensors to measure the movements that occur during gait. To achieve an optimal range of sensor resistance measurements, analog conditioning circuitry utilizes a simple voltage divider with two types of sensors, including a flexible sensor 4.5" in length (flex sensor by Spectra symbol) and two force-sensitive resistors (FSR 402 by Interlink Electronics). A microcontroller (K20P64M72SF1 by Freescale Semiconductor, Inc.) acts as the control center, and can be programmed onboard through a universal serial bus (USB) connection. The analog signals are sampled at 100 Hz via an analog-to-digital

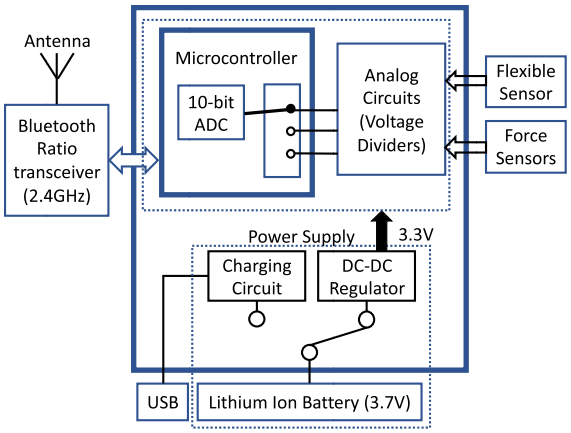

FIGURE 3. Block diagram of the wearable gait monitoring shoe system; the device is capable of wirelessly transmitting data to a remote site (data forwarding).

converter (ADC) with 10-bit resolution on the microcontroller. Electric power is drawn from a single lithium ion battery with a nominal voltage of 3.7 V and a capacity of 500 mAh. The battery can be recharged directly from a USB port by an onboard single-cell lithium ion battery charger (MCP73831 by Microchip). A step-up/step-down charge pump (LTC3240 by Linear Technology) voltage regulator produces a fixed, regulated output of 3.3 V to power the digital devices and peripheral components. The embedded system operates as a data-forwarding device using a 2.4-GHz Bluetooth transceiver module (ZG-B23090W). The ZG-B23090W system uses a regular Bluetooth module based on the CSR BC417 chip with MX 29LV800CBXBI-70G flash memory. Real-time measurements are transmitted to a smart phone with a Bluetooth transceiver. We set the baud rate of the Bluetooth to 115200 bits per second (bps).

B. EXPERIMENTS

Twenty-five participants (nine females: weight 55.8 $\pm$ 5.5 kg, height 160.8 $\pm$ 2.5 cm; 16 males: weight 72.3 $\pm$ 6 kg, height 175.2 $\pm$ 5.5 cm) were involved in experiments for collection of gait data. Among them, 19 participants had flatfoot and six participants had normal foot conditions. These diagnoses were conducted by an expert clinician using the navicular drop test [49], which compares the length from the navicular to the ground between weight-bearing and non-weight-bearing portions of the gait cycle. Each user wore the WGMS on the right foot during the experiment. Participants were asked to walk for five gait cycles, turn around and walk back to the starting point for each data collection. They were asked to walk under five different conditions: tandem walking, walking with step widths matching their pelvic width, walking with a 1.5-cm wedge insole under the front foot, walking with a 1.5-cm wedge insole at the heel, and normal waking.

C. SENSOR SIGNALS

The proposed WGMS generates three signals related to the movements of the toe, heel and ankle, which are essential

FIGURE 4. Gait cycle with the proposed WGMS and five sequential gait steps.

factors in gait movements. In general, the gait process consists of two phases: the stance phase and swing phase. The stance phase is the period when the foot is in contact with the ground. This phase can be determined as the period from heel-strike (HS) to toe-off (TO). The swing phase is the period when the foot is moving above the ground. This can be described as the period from TO to HS. Generally, the stance phase occupies about 60% and swing phase about 40% of the gait process [50], [51]. Fig. 4 shows one gait cycle of a foot equipped with the proposed WGMS. Fig. 5 shows signals from the three sensors over three consecutive gait cycles. It shows that the front and rear force sensors detect the strike or lifting of the toe and heel, and the logical combination of these two events can be used to identify four gait events, namely HS, toe-touch (TT), heel-off (HO) and swing. The flexible sensor provides information about ankle movements, which is segmented by the force sensors.

V. PROPOSED DATA ANALYTICS

A. FEATURE EXTRACTION

In gait event analysis, it is essential to determine the size of the one-unit window that represents a single gait cycle. People have different gait cycle interval times, so the one-unit window size varies from person to person. Some gaits differ based on gait speed and direction. The proposed system defines the one-window length from the typical gait cycle as from one HS to the next HS. To measure this time interval precisely, the rear force sensor is used to identify the exact timing of HS based on rising edge signals of the rear force sensor, which is followed by TT, HO and swing. Fig. 5 (c) shows the filtered signal of the rear force sensor including HS and HO. Fig. 5 (b) shows the filtered signal of the front force sensor including TT and TO. Fig. 5 (d) shows the signal from the flexible sensor, representing dynamic ankle movements. We extracted twelve features from the combined amplitudes and intervals of the gait event factors, as shown in Table 2. The eight intervals considered are from the 1st HS to the 2nd HS, TT, HO, TO, 1st and 2nd flex peaks, and 1st and 2nd flex valleys. We also extracted four amplitudes, representing the first and second peaks and valleys from the flex sensor. These 12 features were the inputs for the preprocessing module described in the next section.

TABLE 2. Intervals and amplitudes extracted from sensor data.

Feature	Name	Symbol	Definition
F1	Heel Strike Interval	HS_i	$2^{nd}HS - 1^{st}HS$
F2	Toe Touch Interval from HS	TT_i	$2^{nd}TT - 1^{st}HS$
F3	Heel Off Interval from HS	HO_i	$2^{nd}HO - 1^{st}HS$
F4	Toe Off Interval from HS	TO_i	$2^{nd}TO - 1^{st}HS$
F5	Flex Sensor 1st Peak Interval from HS	$FP_{1,i}$	$1^{st}P_i - 1^{st}HS$
F6	Flex Sensor 1st Valley Interval from HS	$FV_{1,i}$	$1^{st}V_i - 1^{st}HS$
F7	Flex Sensor 2nd Peak Interval from HS	$FP_{2,i}$	$2^{nd}P_i - 1^{st}HS$
F8	Flex Sensor 2nd Valley Interval from HS	$FV_{2,i}$	$2^{nd}V_i - 1^{st}HS$
F9	Flex Sensor 1st Peak Amplitude	$P_{1,a}$	$1^{st}P_a$
F10	Flex Sensor 1st Valley Amplitude	$V_{1,a}$	$1^{st}V_a$
F11	Flex Sensor 2nd Peak Amplitude	$P_{2,a}$	$2^{nd}P_a$
F12	Flex Sensor 2nd Valley Amplitude	$V_{2,a}$	$2^{nd}V_a$

To extract combined features, we used principal component analysis (PCA) as a preprocessing step prior to classification. PCA is a simple non-parametric method used to extract useful information from complex data [52]. In general, PCA efficiently determines new features that reduce dimensionality and identifies hidden or simplified structures for inclusion in classification algorithms [53]. The data we used in this study consist of the intervals and amplitudes of gait events, and we transformed 23 input features into 12 principal component variables as a preprocessing step using a maximum-attribute filter. Fig. 6 shows the first and second principal components of two different PCAs: (a) a PCA without a scaler and (b) a PCA with a quantile transformer scaler.

B. CLASSIFICATION

Many studies have used deep-learning methods to solve various problems [54]–[61] and many computer-aided diagnosis systems have been developed with deep learning methods for detecting diverse diseases [62]–[71]. We used a DNN with scaled PCA to extract features from the time-series data and identify factors associated with flat feet. Fig. 7 shows the

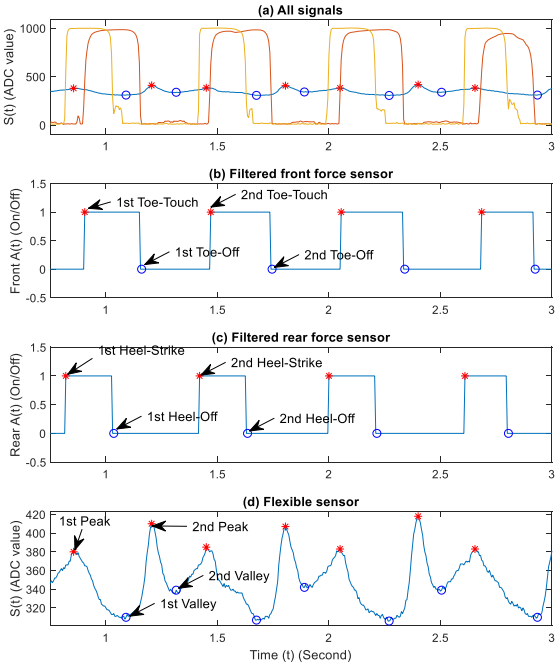

FIGURE 5. Time-series data from the proposed gait monitoring device: (a) all data, (b) filtered front force sensor data, (c) filtered rear force sensor data, and (d) flexible sensor data.

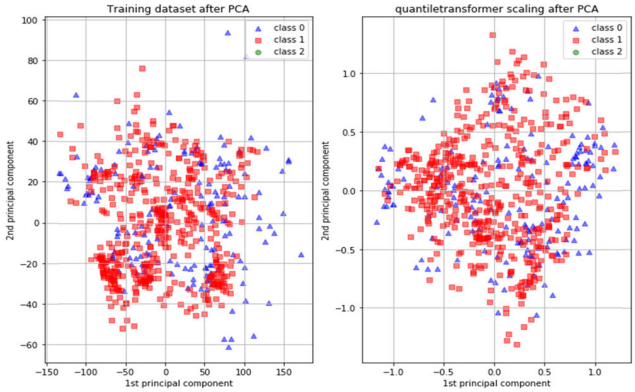

FIGURE 6. Preprocessed features from 12 features using PCA.

proposed DNN architecture: (1) 12 input feature variables were extracted from 24 subjects, and the prepared dataset was divided into training (66%) and testing sets (34%); in the training process, 30% of the training sample was used for validation; (2) PCA and a scaler were applied to convert diverse variables into feature variables as a preprocessing step, and models of the PCA and scaler were generated for testing; (3) we trained the DNN model using the scaled PCA variables; and (4) compared the predicted results with ground truth data provided by clinicians. The testing data were separated from the training data for testing. The overall process is illustrated in Fig. 7.

Statistical assessment of the performance of a binary classification test requires two general performance metrics, sensitivity (*Sn*) and specificity (*Sp*), especially for an imbalanced dataset. If the dataset is balanced, accuracy (*Acc*) alone can reflect the performance of the model. However, our gait dataset is evidently imbalanced; more data points were present for individuals with flat feet (n = 495) than those with non-flat feet (n = 166). Therefore, we used three additional metrics: *Sn*, *Sp* and positive predictive value (*PPV*). *Sn* reflects the probability of detecting flatfoot events, *Sp* indicates the probability of detecting non-flat feet, and PPV is the probability that flatfoot status was correctly classified. We used four status parameters, including true positive (*TP*), true negative (*TN*), false positive (*FP*) and false negative (*FN*), to generate a confusion matrix. *TP* is the number of data points correctly identified as flat feet and the *TN* represents those correctly detected as non-flat feet. *FP* and *FN* are the data incorrectly detected as flat feet and non-flat feet, respectively. *Sn*, *Sp*, *PPV*, and *Acc* can be calculated as follows:

$$Sn = TP/(TP + FN) \tag{1}$$

$$Sp = TN/(TN + FP) \tag{2}$$

$$PPV = TP/(TP + FP) \tag{3}$$

$$Acc = (TP + TN)/(TP + FN + FP + TN) \tag{4}$$

C. DNN ARCHITECTURE

We used a deep learning model including four hidden layers with a simple feed-forward neural network trained using a standard backpropagation algorithm. We adjusted various hyperparameters, including the number of hidden layers, number of neurons in each layer, optimization method, regularization technique and activation function. Among training attempts, the best DNN architecture included four hidden layers with 60 neurons in each layer. An output layer with two neurons generates two regression outputs. We applied regularization terms to the optimization loss function. The proposed DNN includes rectified linear unit (ReLU) activation [72] from all hidden layers, and a dropout probability of 0.1 for each layer [73]. Adam optimization [74] with a learning rate of 0.001 and L2 regularization were used during training. The proposed optimization is robust in terms of hyperparameter selection and showed accurate performance in empirical terms. We applied batch normalization [75] after the first layer to improve performance and stability. The architecture of the proposed DNN is shown in Fig. 8.

VI. RESULTS AND DISCUSSION

We conducted comparative analysis using six classification algorithms: random forest (RF) [76], AdaBoost (ADB) [77], multi-layer perceptron (MLP) [78], Gaussian naive Bayes (GNB) [79], support vector machine (SVM) [80] and our proposed DNN with a min/max scaler. Table 3 shows a summary of the results from the six classification algorithms, including the proposed DNN model. We list thresholds (TH), confusion matrix, and five performance metrics. In Table 3, the area under the curve (AUC) values of the best

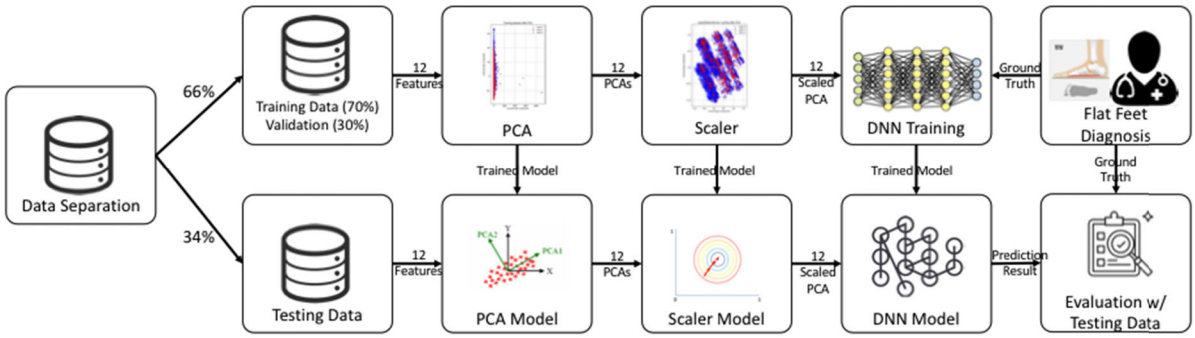

FIGURE 7. The overall integrated architecture of the deep neural network (DNN)/scaled principal component analysis (PCA) approach.

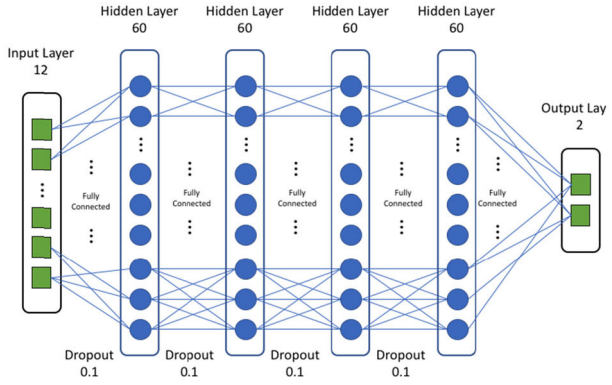

FIGURE 8. The architecture of the proposed DNN.

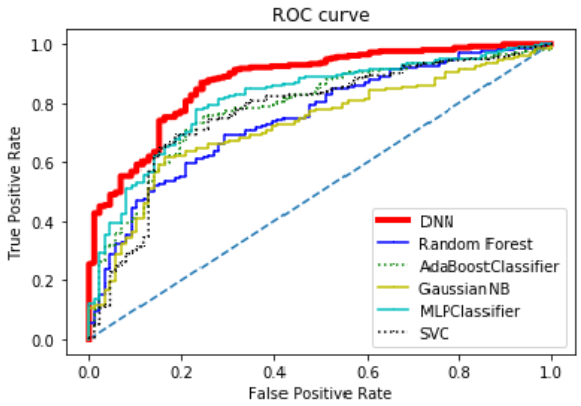

FIGURE 9. Reflecting predictive performance, the area under the receiver operating characteristic curve value was highest (87.1%) for the DNN/scaled PCA classifier.

two classifiers are highlighted in boldface. Considering all model parameters, the optimal threshold of flatfoot probability is 0.92, with an *Acc* of 81.52%, an *Sn* of 83.92%, an *Sp* of 74.42%, and a *PPV* of 90.68%. The thresholds of each classifier were empirically determined to obtain balanced results between sensitivity and specificity. Compared to common performance metrics (*Sn, Sp, PPV,* and *Acc*) used for binary classifiers, *AUC* is a single metric that reflects overall algorithm performance [81]. Fig. 9, a comparison of receiver operating characteristic (ROC) curves of the six classifiers, shows that our model reflects an AUC of 87.1%. The ROC curves indicate that the predictive performance of our DNN/scaled PCA model (bold red line) was best, followed by the MLP classifier (blue line). The better the performance, the closer the ROC curves to the left-upper point [82]. Table 3 and Fig. 9 support the conclusion that the DNN/PCA model with a quantile transformed scaler shows better performance than the other five algorithms. All models were implemented using a Keras [83] and TensorFlow [84] backend. Binary cross entropy served as the loss function for evaluating flat feet detection. As the dataset classes were not balanced, we applied class weighting; this step rendered minority classes more significant.

We determined the correlation coefficients between the measured variables and flat feet. However, the results did not clearly indicate the relationships between principal components and flatfoot occurrence. Table 4 lists the correlation coefficients (r-values) of four variables selected based on r-values over 0.35 among the 12 variables investigated; the strongest correlation (+0.48; Flexible Sensor 2nd Peak Amplitude (f11)) is highlighted in bold and two other strong results (over +/−0.42) are shown in red italics.

We considered tuning hyperparameters, such as the depth of the DNN and the number of nodes, to improve the overall accuracy of flat feet detection. Although optimized hyperparameters are valuable, to the best of our knowledge, there is no general rule for their optimization. We trained 2–8 layers with 10–100 nodes using a trial-and-error method. We used two techniques to minimize the effects of overfitting: dropout and batch normalization. The batch normalization method can avoid loss of feed-forward data, and is appropriate for

TABLE 3. Assessment of selected variables (based on correlation coefficients over 0.35) among 12 variables considered.

	TH	*TP*	*FP*	*FN*	*TN*	*Sn*	*Sp*	*PPV*	*Acc*	*AUC*
RF	0.75	172	27	83	59	67.45	68.60	86.43	67.74	74.78
ADB	0.508	183	20	72	66	71.76	76.74	90.15	73.02	77.13
GNB	0.75	172	28	83	58	67.45	*67.44*	*86.00*	67.45	75.00
MLP	0.786	206	24	49	62	*80.78*	72.09	89.57	78.59	**78.59**
SVC	0.75	191	25	64	61	74.9	70.93	88.43	*73.90*	*74.78*
DNN	0.92	214	22	41	64	83.92	74.42	90.68	81.52	**87.1**

TABLE 4. Correlation coefficients of the variables (over 0.35) among 12 variables.

Variable	Corr. Coeff.	Variable	Corr. Coeff.
F9	*0.420778*	F10	0.355771
F11	**0.488473**	F12	*0.468964*

TABLE 5. Comparison of performance between PCA/DNN and Spectrogram/CNN.

	Sn	*Sp*	*PPV*	*Acc*
Deep learning w/ spectrogram	83.19	76.62	83.93	80.53
DNN w/ PCA	83.92	74.42	**90.68**	81.52

weighting on initialization, while the dropout method uses weighting to minimize the effects of certain nodes in hidden layers.

MLP is a learning algorithm that iteratively learns a set of weights for predicting the class label of tuples. A neural network consists of an input layer, hidden layers, and an output layer. The input layer includes the attributes measured for each training tuple. We set the number of nodes in a hidden layer to be the sum of the number of attributes and classes divided by 2. The initial weights were randomly generated with the seed value 0. The gradient is determined by backpropagation, a neural network-learning algorithm, the learning rate is set to 0.3, and the momentum is set to 0.2. The output biases are updated based on epoch updating and the number of epochs to train through training time were set to 1000. These parameters were found through pilot studies to ensure good performance.

The proposed methodology was compared with the deep learning with the input images of the spectrogram using a short-time Fourier transform. Fig. 10 shows the spectrogram images of two different signals: (a) a normal and (b) one gait cycle of a flat foot. Table 5 shows a comparative result of the proposed DNN with PCA and deep learning with the spectrogram. In Table 5, for similar sensitivities, our proposed method is better than deep learning with spectrogram images in terms of PPV by 6.75%. To implement deep learning with the spectrogram, we convert all gait signals to spectrogram images using MATLAB 2017 and apply the converted images to the web-based image classification tool (Teachable Machine [85]) based on the CNN-based MobileNet [84] with the learning parameters set to 100 epochs, batch-size 64, and learning rate 0.001. Although this methodology eliminates the process of feature extraction, it must transmit its raw data to a computer, so its performance is also slight lower than our proposed method.

The proposed flat foot prediction methodology uses a flexible sensor for measuring ankle movements and force-sensitive resistors for detecting gait cycles. Current studies of wearable devices related to gait analysis use different types of sensors, e.g., force sensitive resistors, air pressure sensors, Wi-Fi signals, accelerometers, IMUs, and their combinations. Sum, *et al.*, (2020) proposed an acceleration-based gait recognition method for older adults and evaluated their

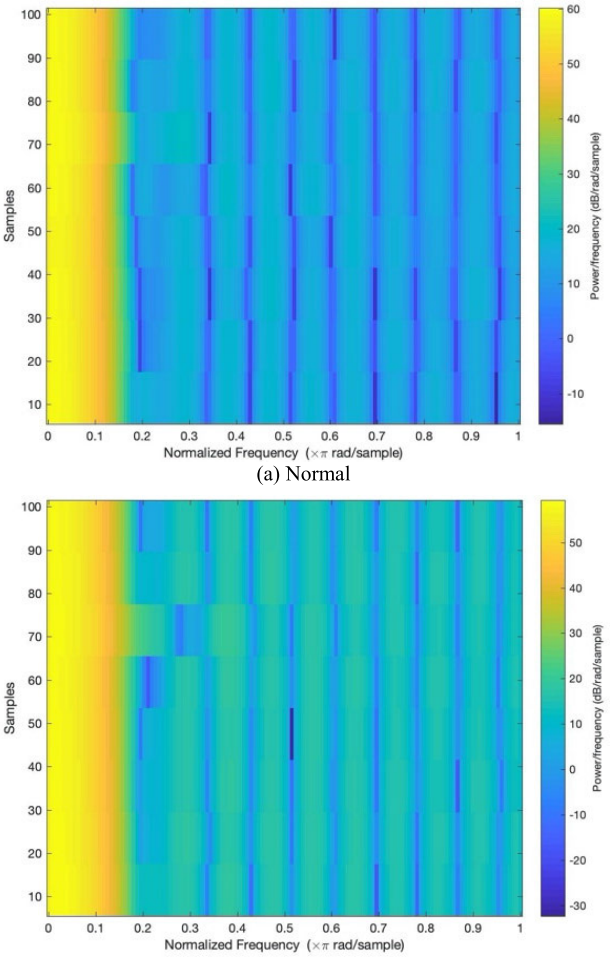

FIGURE 10. Images of the spectrogram using short-time Fourier transform from signals of one gait cycle.

method using a public dataset from 64 older adults [86]. However, the acceleration-based method is somewhat limited to measuring the details of ankle movements. Qiu, *et al.*, (2019) proposed a multi-sensor data-fusion method using a wearable IMU sensor for assessing the gait quality of stroke patients [87]. Although IMU-based sensors are relatively easy to be installed and miniaturized, they are still limited to measuring the details of ankle movements.

Wearable gait-monitoring systems based on force-sensitive resistors and air pressure sensors are similar types of methods that measure the weight and force from gait movement and estimate gait-related features. These methods have advantages in measuring gait cycles and related features because the gait cycle is determined by the force or weight-related features based on whether or not the foot touches the ground. However, ankle movements related to the gait cycles cannot be measured by these types of sensors. Although many sensors embedded in the insole have potential for improving detection accuracy of flat foot detection, too many sensors increase system complexity and energy consumption.

There have been few studies related to prediction of flat-foot based on wearable devices. Wang, *et al.*, (2020) [88] analyzed the effects of the foot pressure sensing insoles for detecting flat feet. Although they provide statistical analysis of features of flat foot and show the possibility of flat foot prediction, detection accuracy of differentiation between the normal group and flat foot group is not provided. Mariani, *et al.*, (2013) [89] used the IMU and pressure insole-based wearable sensors. Although they analyze clinically-meaningful parameters and provide a quantitative estimation of inner-stance phases, prediction of performance, e.g., accuracy of detection between normal vs. abnormal (flat foot), is still not provided. Compared with the studies mentioned above, the proposed flat foot prediction system can provide not only general features of gait but also detailed information about ankle movement, important features for predicting diverse applications of gait-related events.

In the present study, to design an optimal wearable gait monitoring system to be placed within shoes, we designed a pull-on-style, four-way stretch knit sock. The knit-sock shoes are sustainable, as the seamless construction allows digital knitting of the entire upper without material waste [90]. Second, knit socks provide greater comfort than the traditional leather shoes, as they feel similar to lightweight socks. Knitting allows the exact level of flexibility and support to be calculated for every part of the shoe.

VII. CONCLUSION

In this paper, an automatic flat foot detection system based on a WGMS combined with a scaled PCA and DNN is proposed. The WGMS was designed as a pull-on-style wearable and comfortable shoe made from four-way stretch-knit. In the WGMS, an embedded system including two force sensors and one flexible sensor is used to measure the gait and ankle movements, transmitting the signals to a computer for deep learning. Feature extraction and classification based on the scaled PCA and DNN methods were used to detect functional flatfoot. Our methodology allows early detection of individuals at risk of flatfoot who may require additional medical tests and timely treatment to avoid disease exacerbation. The proposed DNN model outperformed five other machine learning models. The results of performance metrics, including Sn, Sp, Pp, Acc and AUC, were 83.92%, 74.42%, 90.68, 81.52% and 87.1%, respectively. Our method can be used to detect functional flatfoot using a wearable device.

We designed the sock-style shoes to provide flexible shoe shapes suitable for carrying the devices and comfortable for users with flat feet. In this study, sex differences and foot shapes were not a primary consideration when designing prototype shoes for flat feet. Therefore, future research should consider sex differences when designing shoes, such as heel width and other essential factors. In addition, the sole design, material, and tread surface area have not been tested to identify how these factors can affect gait and improve grip. Understanding and exploring the user experience is critical to evaluating and improving the product. Therefore, subjecting a prototype to user testing would be beneficial, providing insights from users with flat feet. In addition, in-depth qualitative research, and one-on-one interviews are necessary to identify the factors that affect the individuals wearing the shoes. Finally, as foot anatomy varies among individuals, custom design of shoes using 3D scanning may be another option for creating the best user experience by providing personalized shoes.

ACKNOWLEDGMENT

This study has received IRB approval (YSUIRB-2017-HR-028-02) to allow collection and analysis of sensor data.

REFERENCES

[1] S. Fritz and M. Lusardi, "White paper': Walking speed: 6th vital sign,"' *J. Geriatric Phys. Therapy*, vol. 32, pp. 2–5, 2009.
[2] A. Middleton, S. L. Fritz, and M. Lusardi, "Walking speed: The functional vital sign," *J. Aging Phys. Activity*, vol. 23, no. 2, pp. 314–322, Apr. 2015.
[3] P. Connor and A. Ross, "Biometric recognition by gait: A survey of modalities and features," *Comput. Vis. Image Understand.*, vol. 167, pp. 1–27, Feb. 2018.
[4] C. Wu, F. Zhang, Y. Hu, and K. J. R. Liu, "GaitWay: Monitoring and recognizing gait speed through the walls," *IEEE Trans. Mobile Comput.*, early access, Feb. 19, 2020, doi: 10.1109/TMC.2020.2975158.
[5] A. H. Franco, "Pes cavus and pes planus: Analyses and treatment," *Phys. Therapy*, vol. 67, no. 5, pp. 688–694, 1987.
[6] D. H. Van Boerum and B. J. Sangeorzan, "Biomechanics and pathophysiology of flat foot," *Foot Ankle Clin.*, vol. 8, no. 3, pp. 419–430, Sep. 2003.
[7] R. Marzano, "Functional bracing of the adult acquired flatfoot," *Clinics Podiatric Med. Surg.*, vol. 24, no. 4, pp. 645–656, Oct. 2007.
[8] I. P. I. Pappas, M. R. Popovic, T. Keller, V. Dietz, and M. Morari, "A reliable gait phase detection system," *IEEE Trans. Neural Syst. Rehabil. Eng.*, vol. 9, no. 2, pp. 113–125, Jun. 2001.
[9] I. P. I. Pappas, T. Keller, S. Mangold, M. Popovic, V. Dietz, and M. Morari, "A reliable gyroscope-based gait-phase detection sensor embedded in a shoe insole," *IEEE Sensors J.*, vol. 4, no. 2, pp. 268–274, Apr. 2004.
[10] B. T. Smith, D. J. Coiro, R. Finson, R. R. Betz, and J. McCarthy, "Evaluation of force-sensing resistors for gait event detection to trigger electrical stimulation to improve walking in the child with cerebral palsy," *IEEE Trans. Neural Syst. Rehabil. Eng.*, vol. 10, no. 1, pp. 22–29, Mar. 2002.
[11] Y. Hong and J. X. Li, "Influence of load and carrying methods on gait phase and ground reactions in children's stair walking," *Gait Posture*, vol. 22, no. 1, pp. 63–68, Aug. 2005.
[12] K. Kong and M. Tomizuka, "A gait monitoring system based on air pressure sensors embedded in a shoe," *IEEE/ASME Trans. Mechatronics*, vol. 14, no. 3, pp. 358–370, Jun. 2009.
[13] Y. Blanc, C. Balmer, T. Landis, and F. Vingerhoets, "Temporal parameters and patterns of the foot roll over during walking: Normative data for healthy adults," *Gait Posture*, vol. 10, no. 2, pp. 97–108, Oct. 1999.
[14] J. Rueterbories, E. G. Spaich, and O. K. Andersen, "Characterization of gait pattern by 3D angular accelerations in hemiparetic and healthy gait," *Gait Posture*, vol. 37, no. 2, pp. 183–189, Feb. 2013.
[15] P. Lopez-Meyer, G. D. Fulk, and E. S. Sazonov, "Automatic detection of temporal gait parameters in poststroke individuals," *IEEE Trans. Inf. Technol. Biomed.*, vol. 15, no. 4, pp. 594–601, Jul. 2011.
[16] C. M. Senanayake and S. M. N. A. Senanayake, "Computational intelligent gait-phase detection system to identify pathological gait," *IEEE Trans. Inf. Technol. Biomed.*, vol. 14, no. 5, pp. 1173–1179, Sep. 2010.
[17] F. Alonge, E. Cucco, F. D'Ippolito, and A. Pulizzotto, "The use of accelerometers and gyroscopes to estimate hip and knee angles on gait analysis," *Sensors*, vol. 14, no. 5, pp. 8430–8446, May 2014.
[18] Y. Zhang, K. G. M. Beenakker, P. M. Butala, C.-C. Lin, T. D. C. Little, A. B. Maier, M. Stijntjes, R. Vartanian, and R. C. Wagenaar, "Monitoring walking and cycling of middle-aged to older community dwellers using wireless wearable accelerometers," in *Proc. Annu. Int. Conf. IEEE Eng. Med. Biol. Soc.*, Aug. 2012, pp. 158–161.
[19] S. Tadano, R. Takeda, K. Sasaki, T. Fujisawa, and H. Tohyama, "Gait characterization for osteoarthritis patients using wearable gait sensors (H-gait systems)," *J. Biomechanics*, vol. 49, no. 5, pp. 684–690, Mar. 2016.

[20] S. Yang, J.-T. Zhang, A. C. Novak, B. Brouwer, and Q. Li, "Estimation of spatio-temporal parameters for post-stroke hemiparetic gait using inertial sensors," *Gait Posture*, vol. 37, no. 3, pp. 354–358, Mar. 2013.

[21] D. Gouwanda, "Comparison of gait symmetry indicators in overground walking and treadmill walking using wireless gyroscopes," *J. Mech. Med. Biol.*, vol. 14, no. 1, Feb. 2014, Art. no. 1450006.

[22] D. Gouwanda and S. M. N. Arosha Senanayake, "Identifying gait asymmetry using gyroscopes—A cross-correlation and normalized symmetry index approach," *J. Biomechanics*, vol. 44, no. 5, pp. 972–978, Mar. 2011.

[23] D. Gouwanda and S. M. N. A. Senanayake, "Periodical gait asymmetry assessment using real-time wireless gyroscopes gait monitoring system," *J. Med. Eng. Technol.*, vol. 35, no. 8, pp. 432–440, Nov. 2011.

[24] D. Kotiadis, H. J. Hermens, and P. H. Veltink, "Inertial gait phase detection for control of a drop foot stimulator: Inertial sensing for gait phase detection," *Med. Eng. Phys.*, vol. 32, no. 4, pp. 287–297, 2010.

[25] J. C. Moreno, E. R. de Lima, A. F. Ruíz, F. J. Brunetti, and J. L. Pons, "Design and implementation of an inertial measurement unit for control of artificial limbs: Application on leg orthoses," *Sens. Actuators B, Chem.*, vol. 118, nos. 1–2, pp. 333–337, Oct. 2006.

[26] K. Tong and M. H. Granat, "A practical gait analysis system using gyroscopes," *Med. Eng. Phys.*, vol. 21, no. 2, pp. 87–94, Mar. 1999.

[27] P. Catalfamo, S. Ghoussayni, and D. Ewins, "Gait event detection on level ground and incline walking using a rate gyroscope," *Sensors*, vol. 10, no. 6, pp. 5683–5702, Jun. 2010.

[28] J. K. Lee and E. J. Park, "Quasi real-time gait event detection using shank-attached gyroscopes," *Med. Biol. Eng. Comput.*, vol. 49, no. 6, pp. 707–712, Jun. 2011.

[29] D. Gouwanda and A. A. Gopalai, "A robust real-time gait event detection using wireless gyroscope and its application on normal and altered gaits," *Med. Eng. Phys.*, vol. 37, no. 2, pp. 219–225, Feb. 2015.

[30] K. Ben Mansour, N. Rezzoug, and P. Gorce, "Analysis of several methods and inertial sensors locations to assess gait parameters in able-bodied subjects," *Gait Posture*, vol. 42, no. 4, pp. 409–414, Oct. 2015.

[31] J. M. Jasiewicz, J. H. J. Allum, J. W. Middleton, A. Barriskill, P. Condie, B. Purcell, and R. C. T. Li, "Gait event detection using linear accelerometers or angular velocity transducers in able-bodied and spinal-cord injured individuals," *Gait Posture*, vol. 24, no. 4, pp. 502–509, Dec. 2006.

[32] A. M. Sabatini, C. Martelloni, S. Scapellato, and F. Cavallo, "Assessment of walking features from foot inertial sensing," *IEEE Trans. Biomed. Eng.*, vol. 52, no. 3, pp. 486–494, Mar. 2005.

[33] L. Mertz, "Convergence revolution comes to wearables: Multiple advances are taking biosensor networks to the next level in health care," *IEEE Pulse*, vol. 7, no. 1, pp. 13–17, Jan. 2016.

[34] K. Aminian, B. Najafi, C. Büla, P.-F. Leyvraz, and P. Robert, "Spatio-temporal parameters of gait measured by an ambulatory system using miniature gyroscopes," *J. Biomech.*, vol. 35, no. 5, pp. 689–699, May 2002.

[35] B. Mariani, H. Rouhani, X. Crevoisier, and K. Aminian, "Quantitative estimation of foot-flat and stance phase of gait using foot-worn inertial sensors," *Gait Posture*, vol. 37, no. 2, pp. 229–234, Feb. 2013.

[36] E. Vulcano, J. T. Deland, and S. J. Ellis, "Approach and treatment of the adult acquired flatfoot deformity," *Current Rev. Musculoskeletal Med.*, vol. 6, no. 4, pp. 294–303, Dec. 2013.

[37] N. Shibuya, R. T. Kitterman, J. LaFontaine, and D. C. Jupiter, "Demographic, physical, and radiographic factors associated with functional flatfoot deformity," *J. Foot Ankle Surg.*, vol. 53, no. 2, pp. 168–172, Mar. 2014.

[38] K. A. Johnson and D. E. Strom, "Tibialis posterior tendon dysfunction," *Clin. Orthopaedics Rel. Res.*, vol. 239, pp. 196–206, Feb. 1989.

[39] J. T. Deland, A. Page, I.-H. Sung, M. J. O'Malley, D. Inda, and S. Choung, "Posterior tibial tendon insufficiency results at different stages," *HSS J.*, vol. 2, no. 2, pp. 157–160, Sep. 2006.

[40] J. D. Brodell, A. MacDonald, J. A. Perkins, J. T. Deland, and I. Oh, "Deltoid-spring ligament reconstruction in adult acquired flatfoot deformity with medial peritalar instability," *Foot Ankle Int.*, vol. 40, no. 7, pp. 753–761, Jul. 2019.

[41] M. A. Arnoldner, M. Gruber, S. Syré, K.-H. Kristen, H.-J. Trnka, F. Kainberger, and G. Bodner, "Imaging of posterior tibial tendon dysfunction—Comparison of high-resolution ultrasound and 3T MRI," *Eur. J. Radiol.*, vol. 84, no. 9, pp. 1777–1781, Sep. 2015.

[42] M. S. Lee, J. V. Vanore, J. L. Thomas, A. R. Catanzariti, G. Kogler, S. R. Kravitz, S. J. Miller, and S. C. Gassen, "Diagnosis and treatment of adult flatfoot," *J. Foot Ankle Surg.*, vol. 44, pp. 78–113, 2005.

[43] J. C. Zuil-Escobar, C. B. Martínez-Cepa, J. A. Martín-Urrialde, and A. Gómez-Conesa, "Medial longitudinal arch: Accuracy, reliability, and correlation between navicular drop test and footprint parameters," *J. Manipulative Physiological Therapeutics*, vol. 41, no. 8, pp. 672–679, Oct. 2018.

[44] H. B. Menz, M. E. Morris, and S. R. Lord, "Foot and ankle risk factors for falls in older people: A prospective study," *J. Gerontology A, Biol. Sci. Med. Sci.*, vol. 61, no. 8, pp. 866–870, Aug. 2006.

[45] C. A. Demetracopoulos, P. Nair, A. Malzberg, and J. T. Deland, "Outcomes of a stepcut lengthening calcaneal osteotomy for adult-acquired flatfoot deformity," *Foot Ankle Int.*, vol. 36, no. 7, pp. 749–755, Jul. 2015.

[46] H. S. Shin, J. H. Lee, E. J. Kim, M. G. Kyung, H. J. Yoo, and D. Y. Lee, "Flatfoot deformity affected the kinematics of the foot and ankle in proportion to the severity of deformity," *Gait Posture*, vol. 72, pp. 123–128, Jul. 2019.

[47] A. K. Buldt, S. Forghany, K. B. Landorf, P. Levinger, G. S. Murley, and H. B. Menz, "Foot posture is associated with plantar pressure during gait: A comparison of normal, planus and cavus feet," *Gait Posture*, vol. 62, pp. 235–240, May 2018.

[48] V. Ferraro and S. Ugur, "Designing wearable technologies through a user centered approach," in *Proc. Conf. Designing Pleasurable Products Interfaces (DPPI)*, 2011, pp. 1–8.

[49] J. C. Zuil-Escobar, C. B. Martínez-Cepa, J. A. Martín-Urrialde, and A. Gómez-Conesa, "Medial longitudinal arch: Accuracy, reliability, and correlation between navicular drop test and footprint parameters," *J. Manipulative Physiological Therapeutics*, vol. 41, no. 8, pp. 672–679, Oct. 2018.

[50] J. Perry and J. R. Davids, "Gait analysis: Normal and pathological function," *J. Pediatric Orthopaedics*, vol. 12, no. 6, p. 815, 1992.

[51] M. W. Whittle, *Gait Analysis: An Introduction*. Oxford, U.K.: Butterworth-Heinemann, 2014.

[52] I. T. Jolliffe, "Springer series in statistics," in *Principal Component Analysis*, vol. 29. 2002.

[53] J. Shlens, "A tutorial on principal component analysis," 2014, *arXiv:1404.1100*. [Online]. Available: http://arxiv.org/abs/1404.1100

[54] X. Ma, Z. Dai, Z. He, J. Ma, Y. Wang, and Y. Wang, "Learning traffic as images: A deep convolutional neural network for large-scale transportation network speed prediction," *Sensors*, vol. 17, no. 4, p. 818, Apr. 2017.

[55] K. Xu, D. Feng, and H. Mi, "Deep convolutional neural network-based early automated detection of diabetic retinopathy using fundus image," *Molecules*, vol. 22, no. 12, p. 2054, Nov. 2017.

[56] M. Izadpanahkakhk, S. Razavi, M. Taghipour-Gorjikolaie, S. Zahiri, and A. Uncini, "Deep region of interest and feature extraction models for palmprint verification using convolutional neural networks transfer learning," *Appl. Sci.*, vol. 8, no. 7, p. 1210, Jul. 2018.

[57] O. Steven Eyobu and D. Han, "Feature representation and data augmentation for human activity classification based on wearable IMU sensor data using a deep LSTM neural network," *Sensors*, vol. 18, no. 9, p. 2892, Aug. 2018.

[58] L. Jing, T. Wang, M. Zhao, and P. Wang, "An adaptive multi-sensor data fusion method based on deep convolutional neural networks for fault diagnosis of planetary gearbox," *Sensors*, vol. 17, no. 2, p. 414, Feb. 2017.

[59] M. M. Hassan, M. G. R. Alam, M. Z. Uddin, S. Huda, A. Almogren, and G. Fortino, "Human emotion recognition using deep belief network architecture," *Inf. Fusion*, vol. 51, pp. 10–18, Nov. 2019.

[60] J. Long, Z. Sun, C. Li, Y. Hong, Y. Bai, and S. Zhang, "A novel sparse echo autoencoder network for data-driven fault diagnosis of delta 3-D printers," *IEEE Trans. Instrum. Meas.*, vol. 69, no. 3, pp. 683–692, Mar. 2020.

[61] J. Long, S. Zhang, and C. Li, "Evolving deep echo state networks for intelligent fault diagnosis," *IEEE Trans. Ind. Informat.*, vol. 16, no. 7, pp. 4928–4937, Jul. 2020.

[62] Z. Jiao, X. Gao, Y. Wang, and J. Li, "A parasitic metric learning net for breast mass classification based on mammography," *Pattern Recognit.*, vol. 75, pp. 292–301, Mar. 2018.

[63] Y. Hu, J. Li, and Z. Jiao, "Mammographic mass detection based on saliency with deep features," in *Proc. Int. Conf. Internet Multimedia Comput. Service (ICIMCS)*, 2016, pp. 292–297.

[64] D. Yang, Y. Wang, and Z. Jiao, "Asymmetry analysis with sparse autoencoder in mammography," in *Proc. Int. Conf. Internet Multimedia Comput. Service (ICIMCS)*, 2016, pp. 287–291.

[65] D. Shen, G. Wu, and H. Suk, "Deep learning in medical image analysis," *Annu. Rev. Biomed. Eng.*, vol. 19, pp. 221–248, Jun. 2017.

[66] H.-I. Suk and D. Shen, "Deep learning-based feature representation for AD/MCI classification," in *Proc. Int. Conf. Med. Image Comput. Assist. Intervent.*, 2013, pp. 583–590.
[67] Y.-J. Yu-Jen Chen, K.-L. Hua, C.-H. Hsu, W.-H. Cheng, and S. C. Hidayati, "Computer-aided classification of lung nodules on computed tomography images via deep learning technique," *OncoTargets Therapy*, vol. 8, p. 2015, Aug. 2015.
[68] M. Anthimopoulos, S. Christodoulidis, L. Ebner, A. Christe, and S. Mougiakakou, "Lung pattern classification for interstitial lung diseases using a deep convolutional neural network," *IEEE Trans. Med. Imag.*, vol. 35, no. 5, pp. 1207–1216, May 2016.
[69] D. Kumar, A. Wong, and D. A. Clausi, "Lung nodule classification using deep features in CT images," in *Proc. 12th Conf. Comput. Robot Vis.*, Jun. 2015, pp. 133–138.
[70] Z. Jiao, X. Gao, Y. Wang, and J. Li, "A deep feature based framework for breast masses classification," *Neurocomputing*, vol. 197, pp. 221–231, Jul. 2016.
[71] Z. Jiao, X. Gao, Y. Wang, J. Li, and H. Xu, "Deep convolutional neural networks for mental load classification based on EEG data," *Pattern Recognit.*, vol. 76, pp. 582–595, Apr. 2018.
[72] K. He, X. Zhang, S. Ren, and J. Sun, "Delving deep into rectifiers: Surpassing human-level performance on ImageNet classification," in *Proc. IEEE Int. Conf. Comput. Vis. (ICCV)*, Dec. 2015, pp. 1026–1034.
[73] N. Srivastava, G. Hinton, A. Krizhevsky, I. Sutskever, and R. Salakhutdinov, "Dropout: A simple way to prevent neural networks from overfitting," *J. Mach. Learn. Res.*, vol. 15, no. 1, pp. 1929–1958, 2014.
[74] D. P. Kingma and J. Ba, "Adam: A method for stochastic optimization," 2014, *arXiv:1412.6980*. [Online]. Available: http://arxiv.org/abs/1412.6980
[75] S. Ioffe and C. Szegedy, "Batch normalization: Accelerating deep network training by reducing internal covariate shift," 2015, *arXiv:1502.03167*. [Online]. Available: http://arxiv.org/abs/1502.03167
[76] A. Liaw and M. Wiener, "Classification and regression by randomforest," *R News*, vol. 2, no. 3, pp. 18–22, 2002.
[77] Y. Freund and R. E. Schapire, "A desicion-theoretic generalization of on-line learning and an application to boosting," in *Proc. Eur. Conf. Comput. Learn. Theory*, 1995, pp. 23–37.
[78] M. W. Gardner and S. R. Dorling, "Artificial neural networks (the multilayer perceptron)—A review of applications in the atmospheric sciences," *Atmos. Environ.*, vol. 32, nos. 14–15, pp. 2627–2636, Aug. 1998.
[79] R. Pundlik, "Comparison of sensitivity for consumer loan data using Gaussian Naïve Bayes (GNB) and logistic regression (LR)," in *Proc. 7th Int. Conf. Intell. Syst., Modeling Simulation (ISMS)*, Jan. 2016, pp. 120–124.
[80] S. B. Kotsiantis, I. Zaharakis, and P. Pintelas, "Supervised machine learning: A review of classification techniques," *Emerg. Artif. Intell. Appl. Comput. Eng.*, vol. 160, no. 1, pp. 3–24, 2007.
[81] J. Kim and C.-H. Chu, "ETD: An extended time delay algorithm for ventricular fibrillation detection," in *Proc. 36th Annu. Int. Conf. IEEE Eng. Med. Biol. Soc.*, Aug. 2014, pp. 6479–6482.
[82] F. Chollet, "Keras: The Python deep learning library," ascl, ascl: 1806.022, 2018.
[83] M. Abadi, P. Barham, J. Chen, Z. Chen, A. Davis, J. Dean, M. Devin, S. Ghemawat, G. Irving, M. Isard, and M. Kudlur, "Tensorflow: A system for large-scale machine learning," in *Proc. 12th USENIX Symp. Operating Syst. Design Implement. (OSDI)*, 2016, pp. 265–283.
[84] A. G. Howard, M. Zhu, B. Chen, D. Kalenichenko, W. Wang, T. Weyand, M. Andreetto, and H. Adam, "MobileNets: Efficient convolutional neural networks for mobile vision applications," 2017, *arXiv:1704.04861*. [Online]. Available: http://arxiv.org/abs/1704.04861
[85] M. Carney, B. Webster, I. Alvarado, K. Phillips, N. Howell, J. Griffith, J. Jongejan, A. Pitaru, and A. Chen, "Teachable machine: Approachable Web-based tool for exploring machine learning classification," in *Proc. Extended Abstr. CHI Conf. Hum. Factors Comput. Syst.*, Apr. 2020, pp. 1–8.
[86] F. Sun, W. Zang, R. Gravina, G. Fortino, and Y. Li, "Gait-based identification for elderly users in wearable healthcare systems," *Inf. Fusion*, vol. 53, pp. 134–144, Jan. 2020.
[87] S. Qiu, L. Liu, Z. Wang, S. Li, H. Zhao, J. Wang, J. Li, and K. Tang, "Body sensor network-based gait quality assessment for clinical decision-support via multi-sensor fusion," *IEEE Access*, vol. 7, pp. 59884–59894, 2019.
[88] Y.-T. Wang, J.-C. Chen, and Y.-S. Lin, "Effects of artificial texture insoles and foot arches on improving arch collapse in flat feet," *Sensors*, vol. 20, no. 13, p. 3667, Jun. 2020.
[89] B. Mariani, H. Rouhani, X. Crevoisier, and K. Aminian, "Quantitative estimation of foot-flat and stance phase of gait using foot-worn inertial sensors," *Gait Posture*, vol. 37, no. 2, pp. 229–234, Feb. 2013.
[90] A. Peters. (Mar. 25, 2014). *The Race To Create Knitted Shoes That Cut The Wastefulness Of Our Footwear*. [Online]. Available: https://www.fastcompany.com/3027386/the-race-to-create-knitted-shoes-that-cut-the-wastefulness-of-our-footwear